SUPPLEMENTAL INFORMATION

Supplemental Methods

Crystallization and data collection For crystallization of the XL^{BR-BR} complex, protein complex was mixed with an equal volume of well solution (8-10% isopropanol and 0.1M Bis-Tris pH 5.5). Crystals ($P3_221$, a = 88.1 Å, b = 88.1 Å, c = 43.0 Å) grew at 4°C by hanging drop vapor diffusion. Crystals were washed in well solution and transferred to a cryoprotectant solution containing 10% isopropanol, 0.1M Bis-Tris pH 5.5 and 15% glycerol, then were flash-cooled in liquid nitrogen.

The X1BR2 crystals were grown at 22 °C by hanging-drop vapor diffusion. The X1BR2 was mixed by an equal volume of well solution (10-14% PEG 3350, 0.1M Bis-Tris pH 5.5 and 0.2M $MgCl_2$). Crystals ($P2_12_12_1$, a = 39.0 Å, b = 54.3 Å, c = 101.3 Å) were washed in well solution and transferred to a cryoprotectant solution containing 15% PEG 3350, 0.1M Bis-Tris pH 5.5, 0.2M $MgCl_2$ and 15% glycerol, then were flash-cooled in liquid nitrogen.

The XL^{BR-BR} complex crystals diffracted to 2.9 Å for Se-Met crystals and 2.4 Å for native crystals, and the X1BR2 crystals diffracted to 2.4 Å using synchrotron radiation at the ALS beamline 12.3.1 LBNL Berkeley, California, and there is one XL^{BR-BR} complex and two X1BR2 molecules per asymmetric unit.

Structure determination The XL^{BR-BR} complex structure was solved with MAD (multiple-wavelength anomalous dispersion) using a selenomethionine protein derivative. X-ray data were processed using HKL2000 (1) and Scalepack (1,2). All three SeMet sites were located by automated Patterson searches using SOLVE (3). Experimentally phased maps (Figure S8) had a well-defined solvent boundary and obvious electron density for protein. The crystallographic model was constructed using COOT (4), with refinement in REFMAC (5). TLS parameters were refined using REFMAC, with the L3BR and X1BR2 treated as separate domains. The structure was refined to R of 22.0% and R_{free} of 27.1%. X1BR2 structure was solved with molecular replacement using CNS (6) using X1BR2 structure (7) as a search model. The model was built using COOT (4), with refinement in REFMAC. TLS parameters were refined using REFMAC. The structure was refined to R of 22.0% and R_{free} of 28.1%. 91.1% (for the XL^{BR-BR} complex) and 90.9% (for X1BR2) of residues are found in preferred region. Crystallographic data statistics are shown in Table S1.

Phosphorylation of XRCC1ΔN To phosphorylate XRCC1ΔN, we co-expressed pRSF-trx-XRCC1ΔN-his6 and pGEX-CK2α in *E. coli* Rosetta cells. Thioredoxin(trx)-XRCC1ΔN-his6 was purified by Ni-NTA column and cleaved by precission protease overnight at 4°C. Phosphorylated XRCC1ΔN (XRCC1ΔN-p) was further purified by Superdex 200 gel-filtration column. Both native gel and SDS-PAGE analyses suggest that XRCC1ΔN purified from CK2α-co-expressing *E. coli* cells (XRCC1ΔN-p) was efficiently

phosphorylated as compared to *in vitro* phosphorylated XRCC1ΔN (data not shown). Phosphorylated XRCC1ΔN was digested with trypsin prior to analysis by LC-MS/MS to identify phosphorylation sites. Out of 11 high occupancy phosphorylation sites, 10 were located between the two BRCT domains with 8 sites consistent with previously proposed primary and atypical CK2 target sites in XRCC1 (8).

Ligation and adenylation Assays The concentrations of LigIIIβ and LigIIIα (**Fig. S11A**) were estimated using bovine serum albumin (BSA) as the standard and then corrected by a factor of 2 because of the increased staining of BSA by Coomassie blue. To determine the proportion of pre-adenylated DNA ligase polypeptides in purified preparations, 200 pmol of either Lig IIIβ or LigIIIα/XRCC1 were incubated with 0.5 pmol of a radiolabeled nicked oligonucleotide duplex substrate in a reaction buffer containing 20 mM HEPES-KOH, pH 7.5, 100 mM NaCl, 10 mM $MgCl_2$ and 0.1 mg/ml BSA. Reactions (12 μl final volume) were incubated at 37°C for 12 min prior to the addition of 5 μl of 2% SDS and 5 μl of formamide dye. After heating at 100°C for 5 min, labeled oligonucleotides were separated by denaturing polyacrylamide gel electrophoresis and then detected and quantitated by phosphorimaging using a Typhoon FLA-7000 (GE). As expected, the majority of DNA ligase polypeptides (>55%) were adenylated and Lig IIIβ and LigIIIα/XRCC1 had similar activity under the single turnover conditions (**Fig. S11B**).

Equal amounts (1 μg) of Lig IIIβ and LigIIIα (as part of the LigIIIα/XRCC1 complex) were incubated with 1.6 μCi [α-^{32}P]-ATP (3000 Ci/mmol, Perkin Elmer) in a reaction buffer containing 60 mM Tris-HCl, pH 8.0, 10 mM $MgCl_2$, 5 mM DTT and 50 μg/ml BSA (final volume 15 μl) at 25°C for 15 min. After separation by SDS-PAGE, labeled DNA ligase polypeptides were detected by phosphorimaging using a Typhoon FLA-7000 (GE). Lig IIIβ was more efficiently labeled by [α-^{32}P]-ATP indicating that it has a lower proportion of pre-adenylated molecules compared with LigIIIα/XRCC1 (**Fig. S11C**).

Limited Proteolysis of DNA ligase III Labeled, adenylated Lig IIIβ or LigIIIα (as part of the LigIIIα/XRCC1 complex, 1 μg of each) were incubated with 12.5 ng α-chymotrypsin (Sigma Aldrich) in a reaction buffer containing 40 mM HEPES-NaOH , pH 7.5, 200 mM NaCl, 10% glycerol, 1 mM benzamidine and 0.2 mM PMSF (16 μl final volume) at 25°C for 5 min. Reactions were terminated by the addition of 2 μl of 100 mM 4-(2-aminoethyl)benzenesulfonyl fluoride hydrochchloride, a chymotrypsin inhibitor, (Sigma Aldrich). After separation by SDS-PAGE, labeled DNA ligase polypeptides were detected by phosphorimaging using a Typhoon FLA-7000 (GE).

References

1. Otwinowski, Z. and Minor, W. (1997) In Carter, C. W. and Sweet, R. M. (eds.), *Methods in Enzymology*. Academic Press, New York, Vol. 276, pp. 307-326.
2. Pflugrath, J.W. (1999) The finer things in X-ray diffraction data collection. *Acta Crystallogr D Biol Crystallogr*, **55**, 1718-1725.
3. Terwilliger, T.C. and Berendzen, J. (1999) Automated MAD and MIR structure solution. *Acta crystallographica*, **55**, 849-861.
4. Emsley, P. and Cowtan, K. (2004) Coot: model-building tools for molecular graphics. *Acta Crystallogr D Biol Crystallogr*, **60**, 2126-2132.
5. Murshudov, G.N., Vagin, A.A. and Dodson, E.J. (1997) Refinement of macromolecular structures by the maximum-likelihood method. *Acta Crystallogr D Biol Crystallogr*, **53**, 240-255.
6. Brunger, A.T., Adams, P.D., Clore, G.M., DeLano, W.L., Gros, P., Grosse-Kunstleve, R.W., Jiang, J.S., Kuszewski, J., Nilges, M., Pannu, N.S., Read, R.J., Rice, L.M., Simonson, T. and Warren, G.L. (1998) Crystallography & NMR system: A new software suite for macromolecular structure determination. *Acta Crystallogr. Sect. D Biol. Crystallogr.*, **54**, 905-921.
7. Zhang, X., Morera, S., Bates, P.A., Whitehead, P.C., Coffer, A.I., Hainbucher, K., Nash, R.A., Sternberg, M.J., Lindahl, T. and Freemont, P.S. (1998) Structure of an XRCC1 BRCT domain: a new protein-protein interaction module. *Embo J*, **17**, 6404-6411.
8. Loizou, J.I., El-Khamisy, S.F., Zlatanou, A., Moore, D.J., Chan, D.W., Qin, J., Sarno, S., Meggio, F., Pinna, L.A. and Caldecott, K.W. (2004) The protein kinase CK2 facilitates repair of chromosomal DNA single-strand breaks. *Cell*, **117**, 17-28.

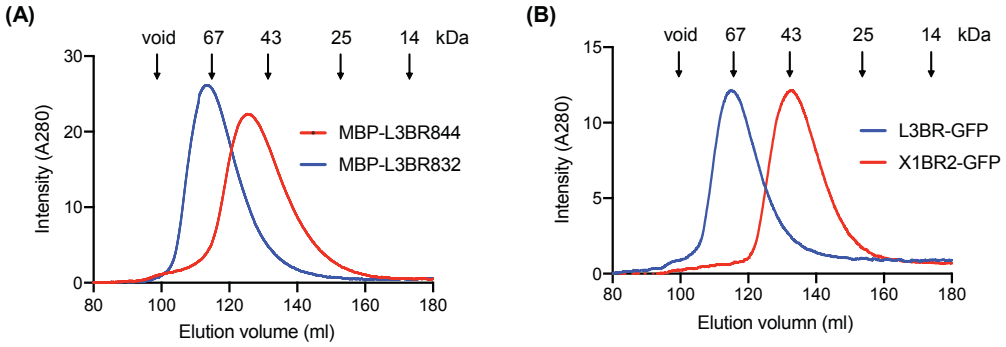

(C)

	Elution Volumn (ml)	MW^{SEC} (kDa)	MW^{seq} (kDa)
MBP-L3BR832	113.5	> 67	51.7
MBP-L3BR844	125.4	50.8	50.3
L3BR-GFP	114.7	> 67	41
X1BR2-GFP	129.8	45.6	41

Figure S1. L3BR N-terminus is required for homodimerization. (**A**) Size-exclusion chromatography (Sephadex 100) of MBP-L3BR832, MBP-L3BR844 (**B**) and L3BR-GFP, X1BR2-GFP. 50 µM of proteins were loaded onto a size exclusion column. (**C**) Molecular weight of protein predicted from sequence (MW^{seq}) and size-exclusion chromatography (MW^{SEC}).

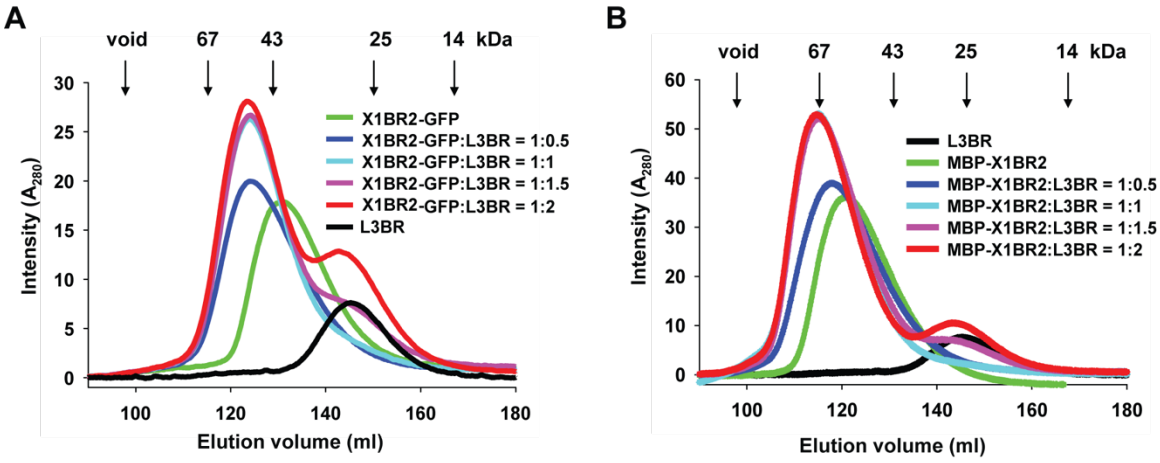

C

	Elution Volumn (ml)	MW^{SEC} (kDa)	MW^{seq} (kDa)
X1BR2-GFP	129.8	45.6	41 (monomer)
X1BR2-GFP + L3BR	122.6	54.2	54 (1:1 ratio)
MBP-X1BR2	121.2	57.4	55 (monomer)
MBP-X1BR2 + L3BR	114.7	68.2	68 (1:1 ratio)
L3BR	145	30.5	13 (monomer)

Figure S2. X1BR2 favorably heterodimerizes with L3BR with 1:1 stoichiometry. A-B. Size-exclusion chromatography (Sephadex 100) of X1BR2-GFP (**A**) and MBP-X1BR2 (**B**). 50 µM of X1BR2 proteins were mixed with increasing amount of L3BR and loaded onto a size exclusion column. **C**. Molecular weight of protein and protein complexes predicted from sequence (MW^{seq}) and size-exclusion chromatography (MW^{SEC}).

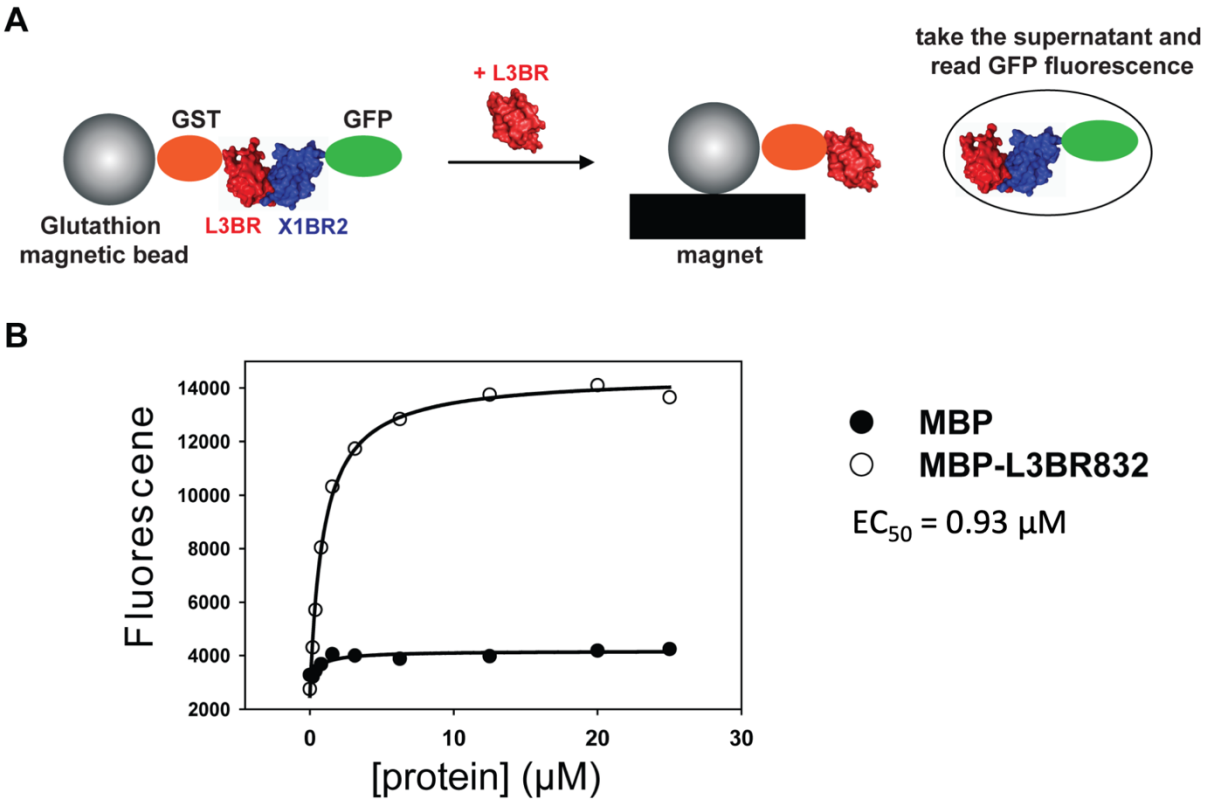

Figure S3. X1BR1 specifically interacts with L3BR. A. GFP-fluorescence-based competition assay. GST-L3BR and X1BR2-GFP complexes are immobilized to GSH-coated magnetic beads. The release of the X1BR2-GFP is monitored by the increased GFP fluorescence of the supernatant after pelleting the beads, as the complex was competed by adding L3BR. **B**. The XL complexes pre-bound to bead were competed by adding MBP and MBP-L3BR832 at the concentration shown. The curve was well fit by a simple hyperbolic 1:1 isotherm, yielding an EC_{50} of 0.93 μM. The data shown represent the mean values and standard deviations from 3 independent experiments.

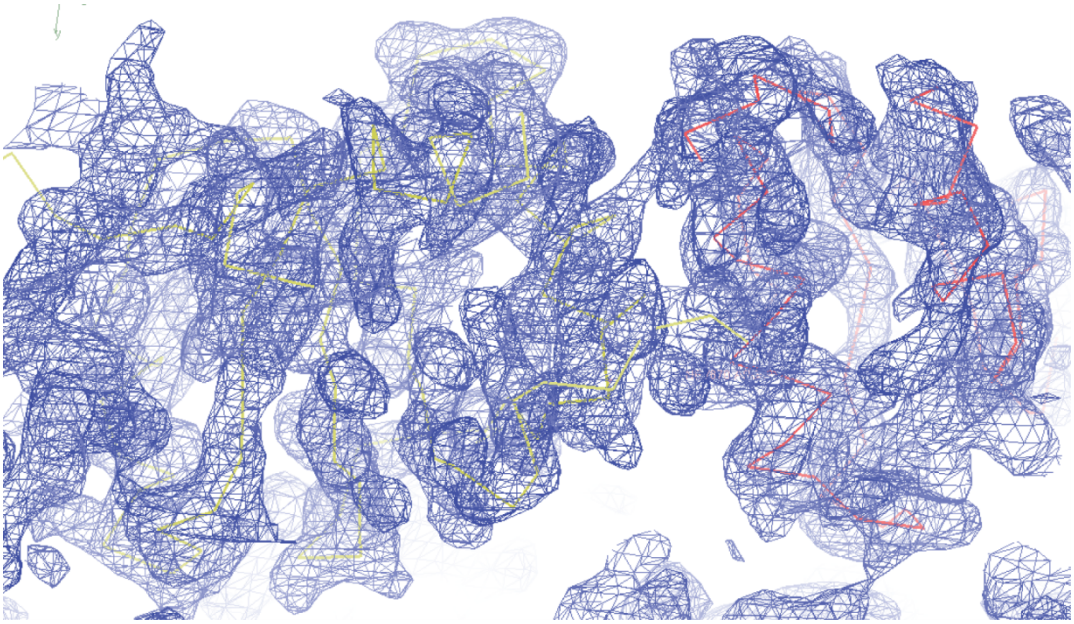

Figure S4. Experimental electron density of human XL^{BR-BR} complex. A 3.0Å resolution MAD-phased electron density of human XL^{BR-BR} complex.

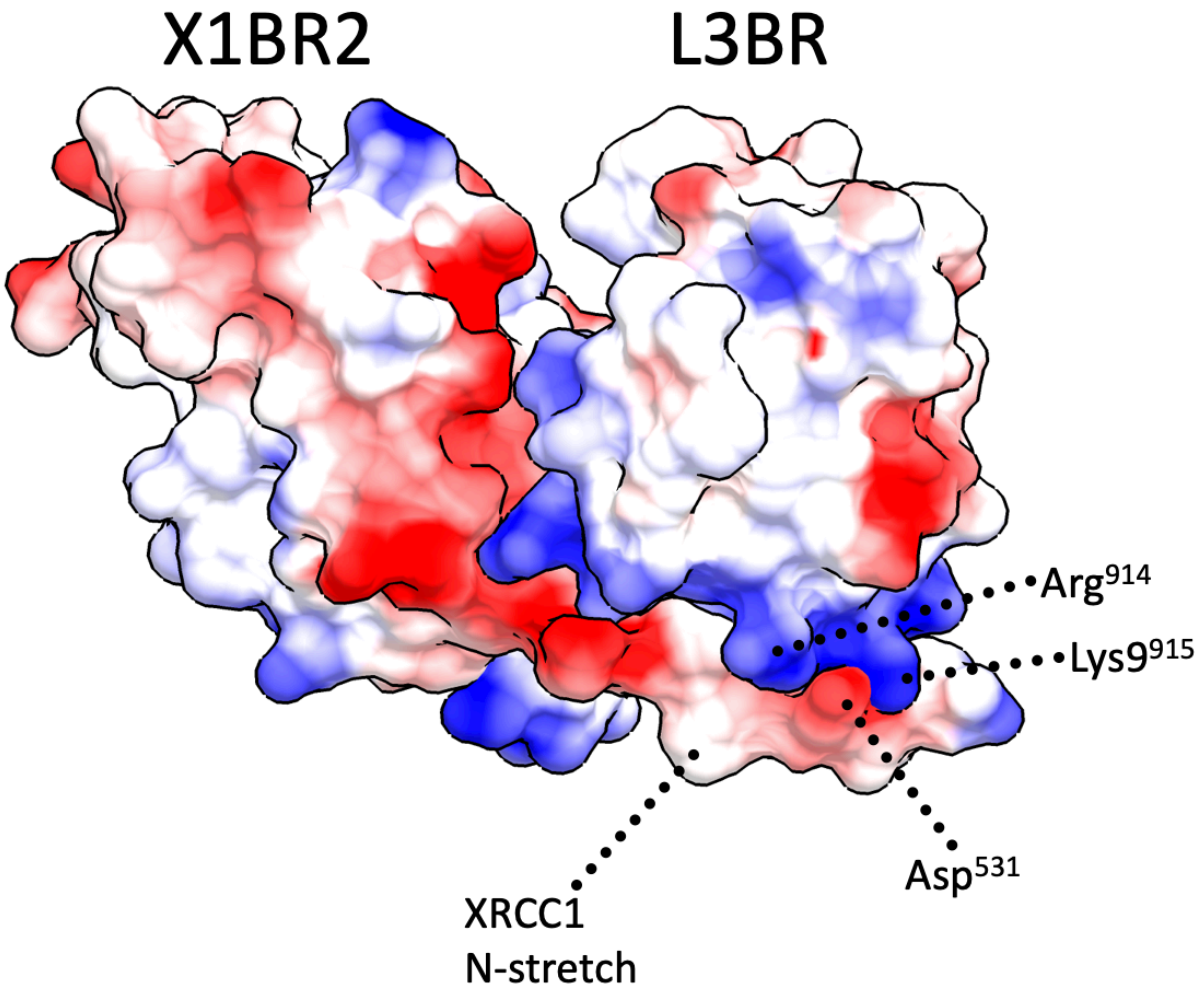

Figure S5. **Electrostatic surface of hybrid XL^{BR-BR} (human X1BR2$^{528-631}$- mouse L3BR $^{841-922}$) complex (PDBID: 3qvg).** Electrostatic interaction between X1BR2^{Asp531} and L3BR$^{Arg914,\ Lys915}$

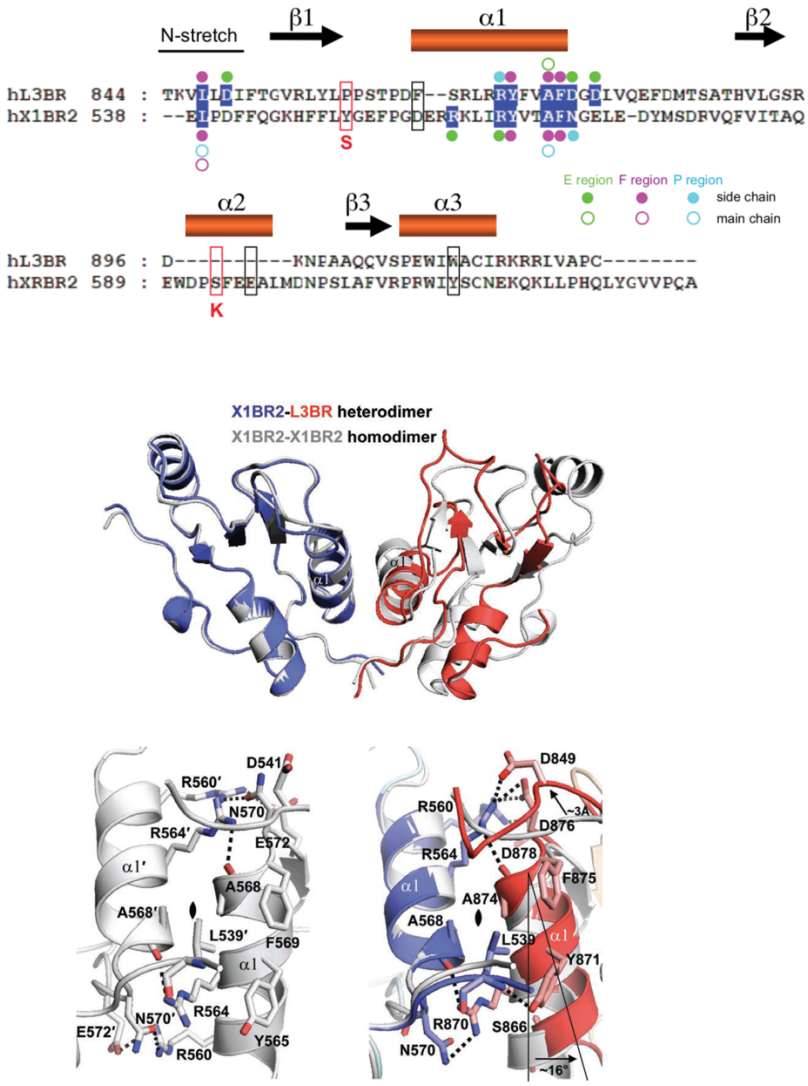

Figure S6. **Sequence alignments of X1BR2 and L3BR with secondary structures.** Top panel, interacting residues of the XL complex are indicated by closed (side chain) and open (main chain) circles (color codes as shown in **Fig. 3A**). The key residues of the conserved PO_4-binding pocket of the tandem BRCT repeats are red-boxed with consensus sequences below. Residues corresponding to pSer(+3)-binding pocket of the tandem BRCT repeats are black-boxed. Middle panel, asymmetry within the $XL^{BR\text{-}BR}$ complex leads to favorable XL heterodimerization. Structural comparison shows a conformational asymmetry of the $XL^{BR\text{-}BR}$ heterodimer with respect to 2-fold symmetric X1BR2 homodimer. One subunit of the X1BR2 homodimer is superimposed onto the X1BR2 subunit of the $XL^{BR\text{-}BR}$ heterodimer. The orientation of the $XL^{BR\text{-}BR}$ complex is same as in **Fig. 3B**. Bottom panel, close view of binding interface of the X1BR2 homodimer that mimics that of the $XL^{BR\text{-}BR}$ heterodimer. Comparison of binding interfaces of the $XL^{BR\text{-}BR}$ heterodimer and X1BR2 homodimer shows the asymmetry of the $XL^{BR\text{-}BR}$ heterodimer strengthens the E- and F-region interactions, leading to favorable XL heterodimerization over homodimerization.

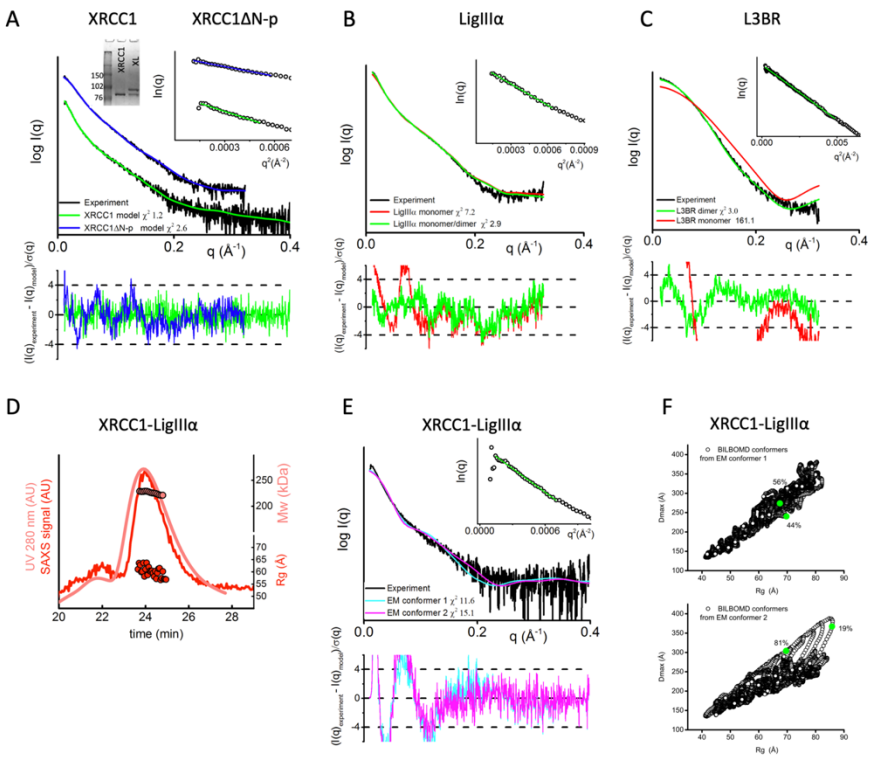

Figure S7. SAXS profiles for XRCC1ΔN-p, XRCC1, LigIIIα, L3BR and XL. A. Inset, purified XL and XRCC1 expressed in sf9 cells. A-C. Experimental (black) and theoretical (colored as indicated) SAXS profiles for the solution state models of XRCC1ΔN-p (see Fig. 1D), XRCC1 (see **Fig.1E**), LigIIIα (see **Fig. 3C**), L3BR crystal structure (PDBID: 3pc7). D. SEC-MALS-SAXS chromatographs for XL complex. Solid lines represent the UV 280nm (light red) or SAXS signal (red) in arbitrary units, while symbols represent molecular mass (light red) and Rg values for each collected SAXS frame (red) versus elution time. E. Experimental (black) and theoretical (colored as indicated) SAXS profiles for the XL dimer as determined by EM (conformer 1 and 2) without linkers regions. (A-C and E) SAXS fits are shown together with the fit residuals in the below graph and Guinier plots for experimental SAXS curves shown in inset. F. Graphs represents the comparison of Rg and Dmax values for all 10,000 XL conformers (black circles) derived by BILBOMD conformational sampling of two initial EM-derived conformers (conformer 1 - top panel, conformer 2 - bottom panel) referenced to the two conformers (green dots) selected by MultiFoXS.

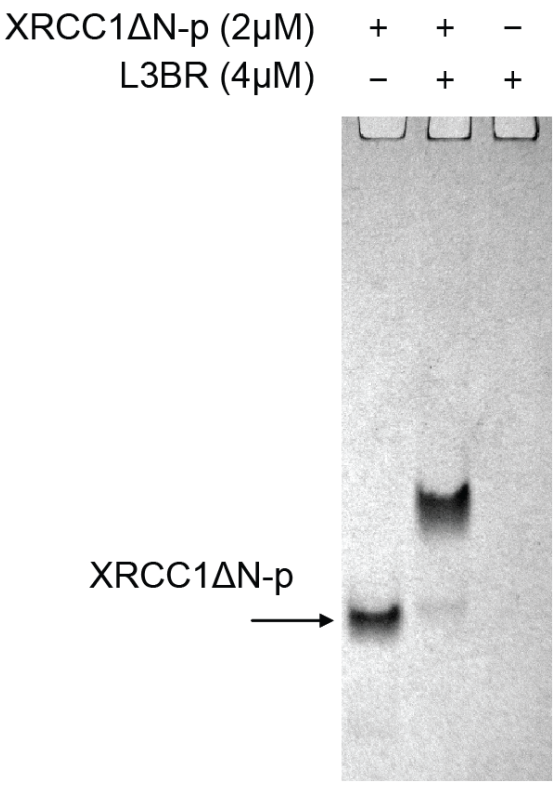

Figure S8. Phosphorylation of XRCC1ΔN does not affect its L3BR binding. Interaction between XRCC1ΔN-p and L3BR was analyzed by native gel analysis. XRCC1ΔN-p (2 μM) was mixed with L3BR (4 μM), and loaded onto 10% native gel.

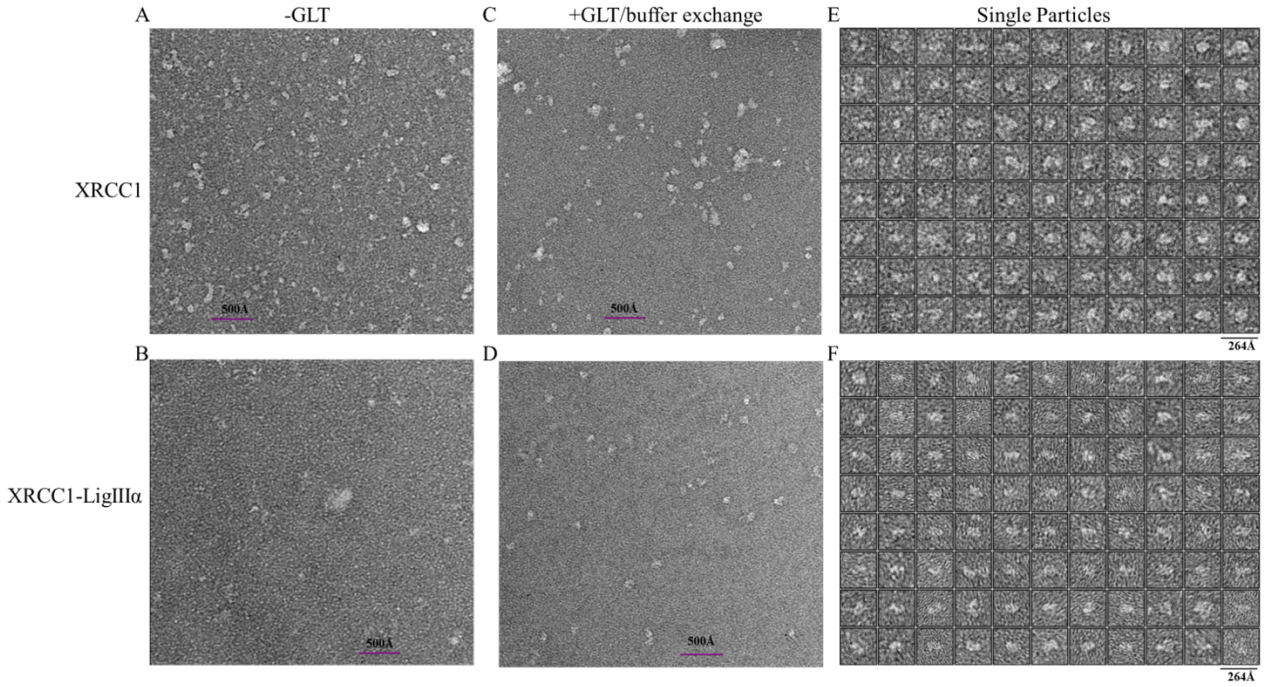

Figure S9. **XRCC1 and XRCC1-LigIIIα particles visualized by negative-stain electron microscopy.** Raw micrographs of XRCC1 (top row) and XRCC1-LigIIIα complex (bottom row) before (A, B) and after (C, D) chemical crosslinking with glutaraldehyde (GLT). The quality of the images improved following crosslinking and buffer exchange into the EM buffer. Single particles for further image processing of XRCC1 (E) were selected from non-crosslinked sample micrographs and the single particles of XRCC1-LigIIIα complex (F) were selected from crosslinked sample micrographs. The lengths of the scale bars and box sizes are indicated.

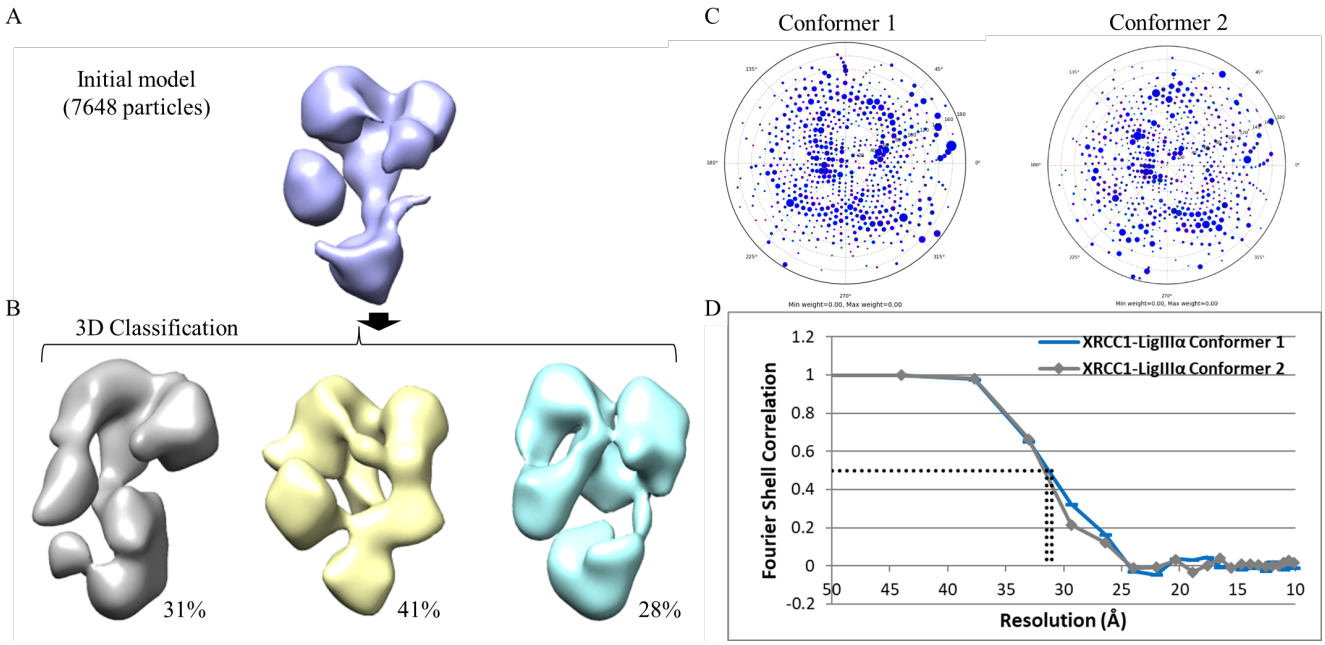

Figure S10. **Modeling of XRCC1-LigIIIα particles visualized by electron microscopy.** The 3D classification and refinement strategy began with an initial model created from single particles (A). This model was used for 3D classification (B) into three classes. Particles belonging to classes 1 and 3 were pooled and used to refine conformer 1. Particles from class 2 were used to create conformer 2. The final refined maps of conformers 1 and 2 show even angular distribution (C) at 31 and 31.5 Å resolution, respectively, as measured by the 0.5 criterion of the Fourier shell correlation (D).

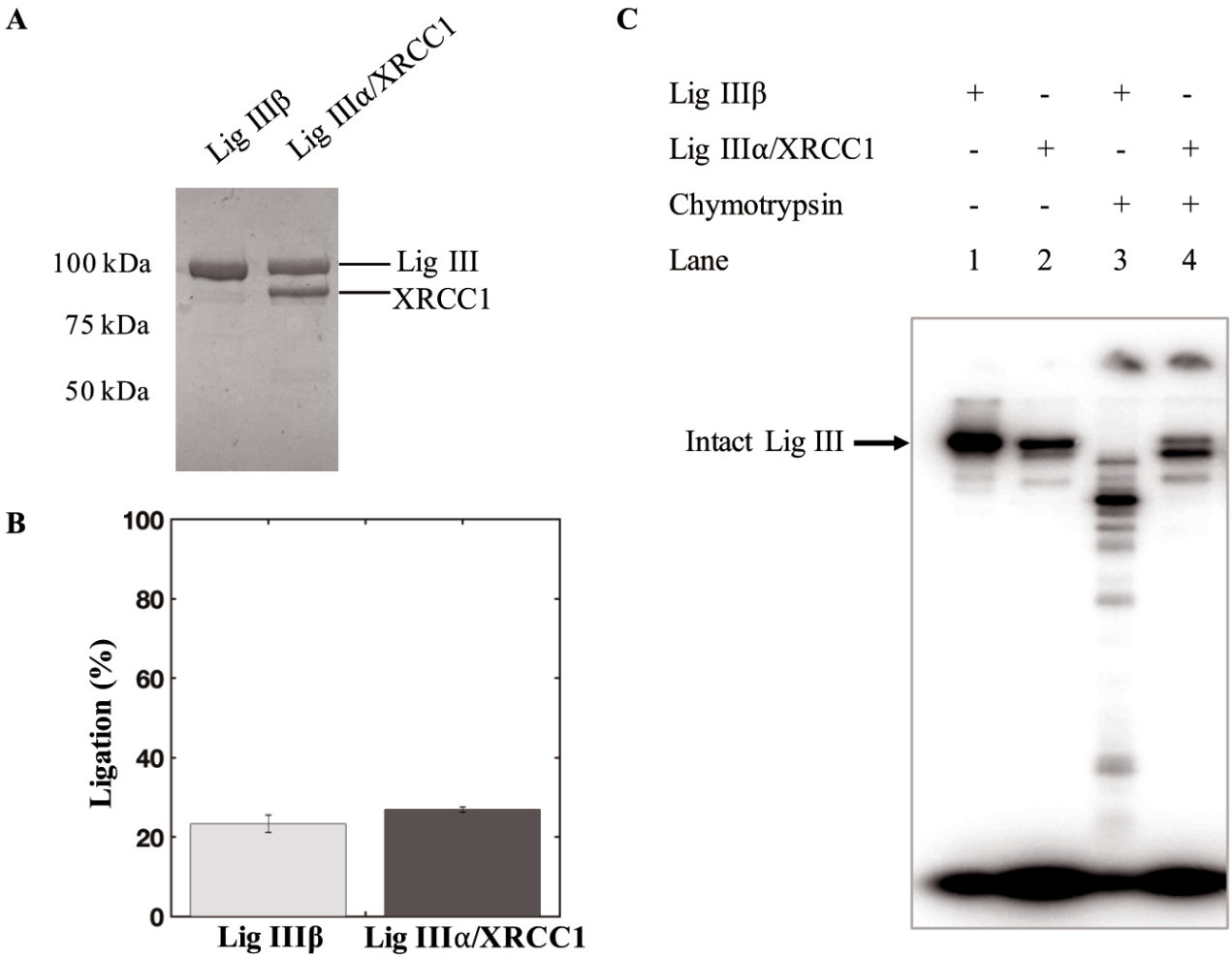

Figure S11. Limited proteolysis of labeled, adenylated LigIII. A. Separation of Coomassie stained SDS-PAGE gel of Lig IIIβ (0.9 μg) and Lig IIIα/XRCC1 (0.6 μg LigIIIα) by SDS-PAGE and then stained with Coomassie blue. **B.** DNA ligation by 200 pmol of either Lig IIIβ or LigIIIα (as part of the Lig IIIα/XRCC1 complex. The results of three independent assays are shown graphically with error bars representing the standard error of the mean. **C**. Lig IIIβ and LigIIIα/XRCC1 were labeled by adenylation as described in Supplemental Methods and then incubated in the absence or presence of chymotrypsin as indicated. A representative gel from three independent experiments is shown.

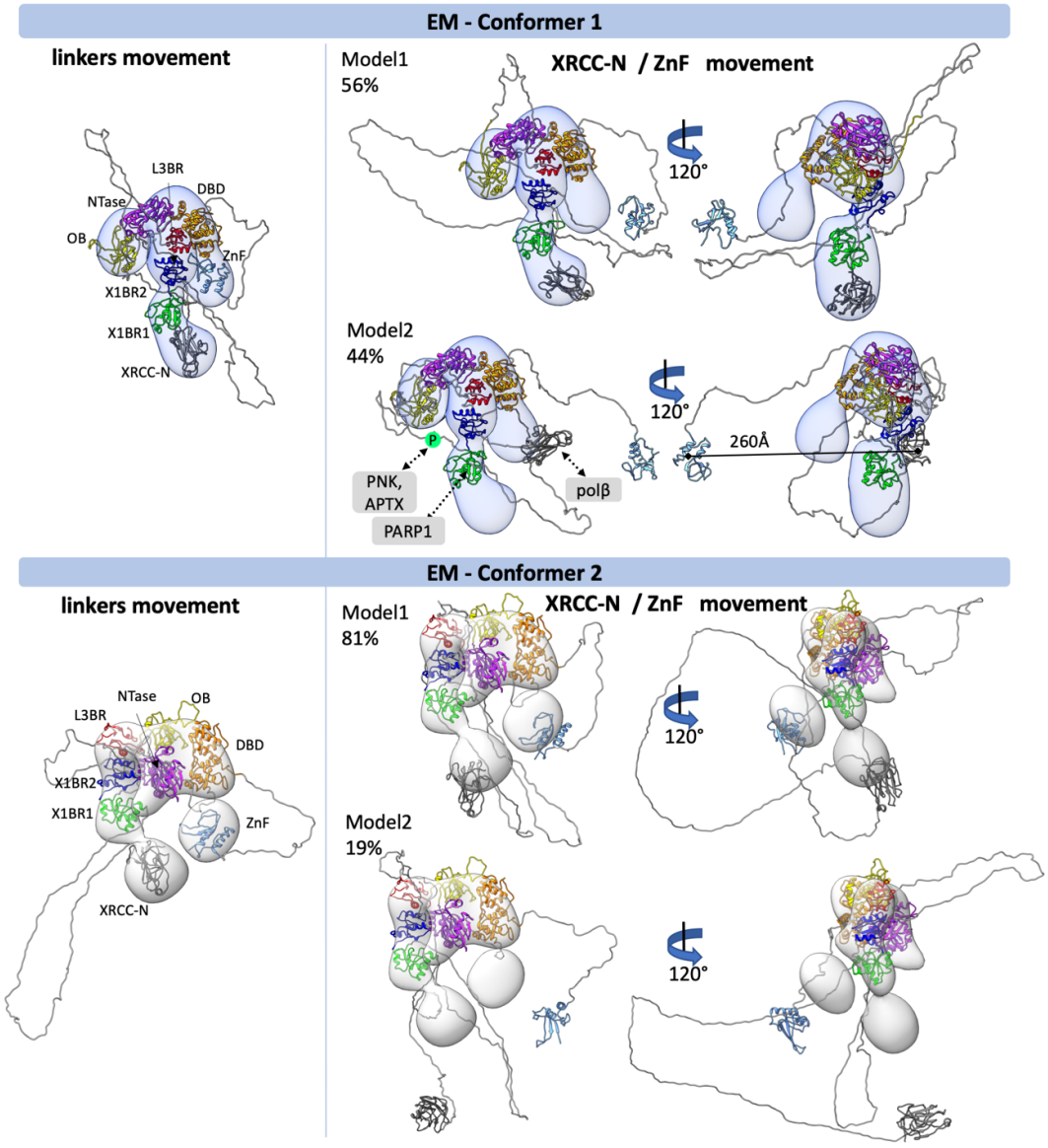

Figure S12. Flexibility of XRCC1-LigIIIα (XL) complex. EM-derived conformers 1 (upper panel) and 2 (lower panel) of XL complex with optimized linker regions (left) compared with the multistate models of the two conformers with the relative contributions of the different species indicated (right). Multistate models of conformers 1 and 2 are shown in two orthogonal views. Atomistic models are superimposed on to the 3D EM maps of conformers 1 and 2. Corresponding SAXS fits for the atomistic models are shown in Fig. 5C and further shown as a theoretical P(r) functions in Fig. 5B. In the upper panel, the binding sites of poly(ADP-ribose) polymerase 1 (PARP1) and DNA polymerase β (polβ) as well as phosphorylation-dependent (Phosphorylation shown as a P in a green circle) binding sites of polynucleotide kinase phosphatase (PNK) and aprataxin (APTX) within XRCC1 are indicated. The N-terminal domain of XRCC1 (XRCC-N) and the N-terminal zinc finger (ZnF) of LigIIIα are shown in the right hand image as being separated by a distance 260Å that was experimentally determined by P(r) function (see Fig. 5B). In the lower panel the flexible tethering of the N-terminal domain of XRCC1 (XRCC-N) and the N-terminal zinc finger (ZnF) of LigIIIα within conformer 2 is highlighted.

Table S1. Crystallographic Data Statistics

Data sets	**X1BR2/L3BR complex** (PDB 6WH1)				**X1BR2** (PDB 6WH2)
	Peak	Inflection	Remote	Native	Native
Space group	$P3_221$	$P3_221$	$P3_221$	$P3_221$	$P2_12_12_1$
Wavelength (Å)	0.96888	0.97964	0.87310	1.12712	1.12712
Resolution (Å)	20-2.9	20-2.9	20-2.9	20-2.4	20-2.4
Completeness (%)[a]	99.9	99.8	99.7	98.4	98.2
R_{sym} (%)[a,b]	3.1 (38.6)	3.1 (41.0)	3.6 (56.1)	4.1 (47.7)	4.9 (26.0)
Average I/σ	35.9 (3.1)	32.8 (2.4)	26.1 (1.6)	29.9 (2.4)	18.3 (3.2)
Refinement statistics					
Resolution range (Å)				20-2.4	20-2.4
Number of reflections				38,025	31,392
Total number of atoms					
Total				1425	1652
Water				37	39
Completeness of data (%)				98.4	98.2
R^c (R_{free}) (%)				22.1 (27.2)	22.1 (28.1)
r.m.s. deviations[d]					
Bonds (Å)				0.019	0.017
Angles (°)				1.79	1.55

[a] The number in parentheses is for the outer shell.
[b] $R_{sym} = \Sigma_h\Sigma_I|I_{h,i} - I_h|/\Sigma_h\Sigma_I I_{h,i}$, where I_h is the mean intensity of the i observations of symmetry related reflections of h.
[c] $R = \Sigma|F_o-F_c|/\Sigma F_o$, where $F_o = F_p$, and F_c is the calculated protein structure factor from the atomic model. R_{free} was calculated with 10% of the reflections.
[d] Root mean square (r.m.s.) deviations in bond length and angles are the deviations from ideal values.

Table S2. Structural parameters from SAXS and MALS data

SAXS sample (SASDBD ID)	D_{max} (Å)	R_g (Å)	MW Seq. monomer (kDA)	MW SAXS (kDa)	MW MALS (kDa)	Model fit $\chi 2$
LigIIIα (SASDJ72)	~ 200	61.0 ± 0.6	102	130-150	ND	2.9
[a]XRCC1 (SASDJ62)	~ 230	45 - 65	70	100-135	70-110	1.2
[b]XRCC1/LigIIIα (SASDJ82)	~ 250	62.2 ± 1.8	180	180	215	1.6
L3BR	~ 80	21.1 ± 0.1	10	21	ND	3.0
XRCC1ΔN (SASDJ52)	~ 200	55.3 ± 0.6	39	82	ND	ND
XRCC1ΔN-p	~ 200	54.2± 0.3	39	83	ND	2.7
XRCC1ΔN-p/L3BR	~ 225	56.4 ± 0.6	49	96	ND	ND

[a] 4.3 mg/ml 6His-XRCC1 in 200 mM NaCl, 20 mM Tris-HCl, pH 7.5 , 2% Glycerol

[b] 5.96 mg/ml Strp- LigIIIα/6His-XRCC1 in 50 mM Tris-HCl, pH 7.5, 100 mM NaCl, 5 mM $MgCl_2$, 0.2 mM PMSF, 1 mM Benzamidine.